How to cite: *Angew. Chem. Int. Ed.* **2022,** *61,* e202201610
International Edition: doi.org/10.1002/anie.202201610
German Edition: doi.org/10.1002/ange.202201610

Oxygen Evolution

Dual In Situ Laser Techniques Underpin the Role of Cations in Impacting Electrocatalysts

Shujin Hou, Lili Xu, Xing Ding, Regina M. Kluge, Theophilus Kobina Sarpey, Richard W. Haid, Batyr Garlyyev, Soumya Mukherjee, Julien Warnan, Max Koch, Shengli Zhang, Weijin Li,* Aliaksandr S. Bandarenka,* and Roland A. Fischer**

Abstract: Understanding the electrode/electrolyte interface is crucial for optimizing electrocatalytic performances. Here, we demonstrate that the nature of alkali metal cations can profoundly impact the oxygen evolution activity of surface-mounted metal–organic framework (SURMOF) derived electrocatalysts, which are based on NiFe(OOH). In situ Raman spectroscopy results show that Raman shifts of the Ni–O bending vibration are inversely proportional to the mass activities from Cs^+ to Li^+. Particularly, a laser-induced current transient technique was introduced to study the cation-dependent electric double layer properties and their effects on the activity. The catalytic trend appeared to be closely related to the potential of maximum entropy of the system, suggesting a strong cation impact on the interfacial water layer structure. Our results highlight how the electrolyte composition can be used to maximize the performance of SURMOF derivatives toward electrochemical water splitting.

To accelerate the necessary transition to "green", renewable energy systems, designing efficient electrochemical devices such as electrolyzers, fuel cells, or metal–air batteries is of paramount importance.[1] Further optimization of such electrocatalytic systems greatly relies on the engineering of electrocatalysts and the understanding of the electrode/electrolyte interface processes.[2] Recently, NiFe(OOH) catalysts derived from the structural metamorphosis of surface-mounted metal–organic frameworks (SURMOFs) have shown record mass activities towards the oxygen evolution reaction (OER).[3] The metamorphosis of the SURMOF precatalyst offers key advantages here, such as ultra-thin coatings with low mass loading, no binder or additives, and kinetically driven active catalyst structures. Together, these aspects enable to achieve a high density of accessible active sites. This led us to select SURMOF-derived NiFe(OOH) catalysts for our study. Previous studies have focused on identifying the active sites and species in MOF-based catalytic systems and discovering the transformation mechanisms as well as the structure-functionality correlations under various environments. As an outcome, factors like electrolyte pH, temperature, electric field, and nature of the binder are of particular importance.[4] However, the influence of those factors on the electrochemical interface remained unclear in most cases.

Electrolyte cations, such as Li^+, Na^+, K^+, and Cs^+, have been proven to significantly influence the OER activity through the non-covalent interactions between hydrated cations and adsorbed reactants or reaction intermediates at the electrode/electrolyte interface.[5] The activity typically increases with cation size, which is tightly associated with the hydration energies, electronegativities, and Lewis acidities.[5,6] However, the specific nature of the cation effects in the electrocatalytic OER remains indeterminate, as it is not trivial to perform the necessary experiments, and it is still little experimental information available to build a strong well-supported and verified theory. In

[*] S. Hou, X. Ding, Dr. R. M. Kluge, T. K. Sarpey, R. W. Haid, Dr. B. Garlyyev, Prof. A. S. Bandarenka
Physics of Energy Conversion and Storage,
Department of Physics, Technical University of Munich
James-Franck-Straße 1, 85748 Garching (Germany)
E-mail: bandarenka@ph.tum.de

S. Hou, Dr. S. Mukherjee, Dr. J. Warnan, Dr. W. Li, Prof. A. S. Bandarenka, Prof. R. A. Fischer
Catalysis Research Center, Technical University of Munich
Ernst-Otto-Fischer-Straße 1, 85748 Garching (Germany)

Dr. S. Mukherjee, Dr. J. Warnan, Dr. W. Li, Prof. R. A. Fischer
Chair of Inorganic and Metal–Organic Chemistry,
Department of Chemistry, Technical University of Munich
Lichtenbergstraße 4, 85748 Garching (Germany)
E-mail: roland.fischer@tum.de
wj.li@tum.de

L. Xu, Prof. S. Zhang, Dr. W. Li
Institute of Optoelectronics & Nanomaterials,
College of Materials Science and Engineering,
Nanjing University of Science and Technology
Nanjing 210094, Jiangsu (China)
E-mail: zhangslvip@njust.edu.cn

M. Koch
Department of Chemistry, Technical University of Munich
Lichtenbergstraße 4, 85748 Garching (Germany)

essence, the key problems with reoccurring discrepancies in cation effects remain. Michael et al.[7] pointed out that the activity of NiOOH in purified electrolytes follows the trend of $Cs^+ > K^+ \approx Na^+ \approx Li^+$, which is closely related to the length of the Ni–O bonds in the NiOOH active-phase structure. By contrast, Garcia et al.[8] stated a different trend in the cation enhancement effect on the OER activity of NiOOH, namely, $Cs^+ > Na^+ > K^+ > Li^+$. Although extensive studies suggest that at the electrode/electrolyte interface, the interaction between electrolyte cations and adsorbed intermediate species plays a pivotal role in the catalytic activity, the deeper interfacial mechanisms are not entirely understood. For instance, in the alkali metal group, the smaller cations with high electronegativities remarkably influence the hydration shells as well as the interfacial water structure by the stronger non-covalent interaction. The looseness and reorientation time of interfacial water molecules enable modification of the reaction kinetics, however, there is a limited understanding regarding the cation effect on the electric double layer (EDL) structure. Systematic investigation of this effect and development of activity descriptors governing the reaction kinetics are imminent.

Under this backdrop, herein, we investigate the influence of the electrolyte composition on the performance of state-of-the-art SURMOF-derived OER electrocatalysts by employing in situ Raman spectroscopy and a profound methodology called laser-induced current transient (LICT) technique.[9] Our results indicate that the activity increase in the order $Cs^+ > K^+ > Na^+ > Li^+$ follows an opposite trend as the Raman shifts, suggesting a strong interaction between the interfacial cations and the reaction intermediates. Moreover, the LICT technique can access the potential of maximum entropy (PME) related to the EDL structure and the interfacial energy barriers for electrochemical reactions.[9a] The degree of order of the interfacial water molecules (rigidity or looseness) could affect the movement of reactants and block the contact with catalytically active sites.[10] In other words, the closer the PME of the material is to the thermodynamic equilibrium potential of the OER, the faster the reaction rate will be. The PMEs of the SURMOF derived materials were measured in the presence of different alkali metal cations. Our results indicate that different alkali metal cations indeed shift the PME and consequently change the OER performance. The cation-dependence of the OER activity is in line with the trend of the PMEs. Therefore, this work analyzes the cation enhancement effect on the OER from various research perspectives and highlights the importance of electrode/electrolyte interface engineering in the design of highly active electrocatalysts.

The transformation process of the as-prepared SURMOFs to the electrocatalytically active derivatives is schematically illustrated in Figure 1 (details are available in the Materials and Methods section of the Supporting Information). Typically, the heterostructured Ni|Fe-[TA]-SURMOFs (where [TA] stands for the deprotonated terephthalic acid) were synthesized via a tandem process. This involved the vertical growth of 2D Ni-[TA] nanosheets on surface-functionalized quartz crystal microbalance (QCM) gold substrates followed by the deposition of Fe-[TA] nanospheres as the top layer of the SURMOFs.

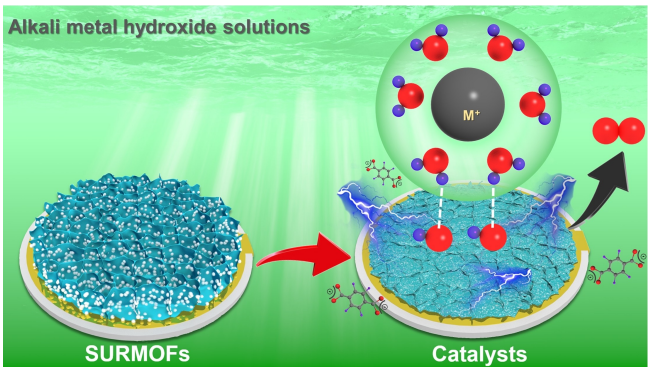

Figure 1. Schematic illustration of the cation effect. It depicts the structural transformation of heterostructured Ni|Fe-[TA]-SURMOFs into highly active OER catalysts and the effect of hydrated alkali metal cations on the OER via non-covalent interactions with the adsorbed OH-species. Here, the electrolytes containing different alkali metal cations are denoted as MOH ($M^+ = Li^+$, Na^+, K^+, Cs^+). Color scheme: oxygen in red, hydrogen in blue, and alkali metal cation (M^+) in black.

The as-prepared Ni|Fe-[TA]-SURMOFs precursors undergo a structural transformation into Ni|Fe-[TA]-derived catalysts during the alkali immersion treatment and subsequent electrochemical activation. Note that the SURMOFs after electrochemical cycling are hereafter denoted as "Catalysts". As shown in our previous work,[3a,c] this process results in highly active NiFe-hydroxide electrocatalysts and the partial leaching of organic linkers from the pristine SURMOFs. Moreover, the proposed interaction between the hydrated alkali metal cations and the adsorbed OH-species on the electrode surface is schematically described in Figure 1 according to the previously reported non-covalent interaction model.[6a]

To investigate the surface morphology of the SURMOFs and their derivatives, scanning electron microscopy (SEM) was used. For the heterostructured Ni|Fe-[TA]-SURMOFs, Fe-[TA] nanoparticles are observed on the surface of Ni-[TA] nanosheets from the top-view and cross-section SEM images (Figure S2). After electrochemical cycling, the network morphologies of the derived catalysts are entirely different from the heterostructure of the pristine SURMOFs (Figure S3), validating the hypothesis of a structural transformation. In contrast, the alkaline electrolytes have little influence on the surface morphology and the contents of Ni and Fe for the derived catalysts (Table S3). Furthermore, grazing incidence X-ray diffraction (GIXRD) was used to characterize the changes in the crystalline structure. As shown in Figure S4a, the pronounced peaks of the as-prepared SURMOFs match well with the simulated XRD patterns, in accordance with the literature reports.[11] However, the peaks associated with the crystalline phase disappeared after electrochemical cycling in the presence of different alkali metal cations (Figure S4b), signifying the phase transition of the crystalline SURMOFs into amorphous derivatives. To further clarify the transformation

mechanism, X-ray photoelectron spectroscopy (XPS) was conducted to ascertain the differences in surface chemical states and the chemical compositions of the samples before and after the structural changes. A similar conclusion can be drawn that the electrochemical activation in alkaline electrolytes results in component reconstruction and linker leaching from the pristine SURMOFs. (More descriptions regarding the XPS data are shown in the Supporting Information) The characterization substantiates the transformation of the heterostructured SURMOF precursors into a low-crystallinity NiFe(OOH)-type electrocatalyst.

The electrocatalytic performance of the as-prepared samples was evaluated in O_2-saturated 0.1 M MOH electrolytes (M stands for the alkali metal cations) using the three-electrode configuration. All the OER polarization curves were normalized to the derived catalyst's mass, recorded using a 5 MHz QCM electrode. Before the OER test, the SURMOF electrodes were immersed into their respective electrolytes for 3 min, and the cyclic voltammetry (CV) was measured at a scan rate of 20 $mV\,s^{-1}$. This is done to facilitate the structural transformation of SURMOFs into NiFe(oxy)hydroxides.[12] As shown in Figure S6, all CVs (no iR correction) display a similar activation process behavior where the Ni^{3+}/Ni^{2+} redox couple currents increase from the 1st to 35th cycles and stabilize subsequently. This result indicates the conversion from the SURMOF structure to an electrochemically stable material. Electrochemical cycling achieves the successive exposure of Ni^{2+} to Ni^{3+} species and increases the number of accessible active sites.[12] Moreover, the mass loading on the QCM electrode was dramatically reduced to ca. 68 % of its initial value after the OER test (Figure S7) for all electrolytes, attributed to the dissociation of organic linkers from the SURMOFs. The OER electrocatalytic performance of the derived catalysts was measured in the corresponding LiOH, NaOH, KOH, or CsOH electrolytes (at a concentration of 0.1 M) (Figure 2a). The effect of alkali metal cations on water oxidation performance can be observed following an activity trend of $Cs^+ > K^+ > Na^+ > Li^+$, which is in good accordance with the previous reports.[13] As shown in Figure 2b, the corresponding approximated Tafel slopes increase in the order of Cs^+ ($\approx$72 $mV\,dec^{-1}$) < K^+ ($\approx$78 $mV\,dec^{-1}$) < Na^+ ($\approx$79 $mV\,dec^{-1}$) < Li^+ ($\approx$96 $mV\,dec^{-1}$). In Figure 2c, the Ni|Fe-[TA]-Catalyst exhibits a remarkable mass activity of $\approx$0.80 $kA\,g^{-1}$ at 1.53 V vs. RHE in CsOH, which is nearly 1.1, 1.3, and 2.2 times higher than the mass activities in KOH, NaOH, and LiOH, respectively. For the enhancement effect due to the cations, literature reports suggested that hydrated alkali metal cations in the form of OH_{ad}–$M^+(H_2O)_n$ or OH_{ad}–(H_2O)–$M^+(H_2O)_n$ clusters can interact with the adsorbed OH-species at the interface between the electrolytes and catalysts via non-covalent bonds.[6a] The interaction is directly proportional to the hydration energies of metal ions. Typically, the smallest cation with the largest hydration energy exhibits the strongest interaction with the electrode surface, thus preventing some reactants from reaching the active sites. As shown in Figure 2d, one can find that the increase of OER electrocatalytic activities from Li^+ to Cs^+ is strongly correlated with the decreasing hydration energies, which is also in good agreement with the literature.[13a]

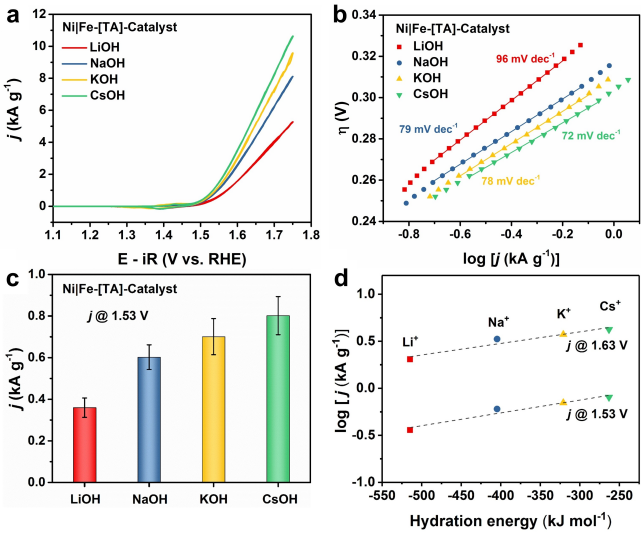

Figure 2. Electrocatalytic performance. a) OER polarization curves of the Ni|Fe-[TA]-Catalysts recorded in O_2-saturated 0.1 M LiOH (pH 12.9), 0.1 M NaOH (pH 13.1), 0.1 M KOH (pH 13.2), and 0.1 M CsOH (pH 13.3) electrolytes. Scan rate, 5 $mV\,s^{-1}$. b) Corresponding Tafel plots. c) Comparison of the catalyst mass activities at 1.53 V vs. RHE in different electrolytes. d) Electrocatalytic activities obtained at 1.53 V and 1.63 V vs. RHE as a function of alkali metal cation hydration energies.

To gain deeper insight into the above-determined experimental trend, we used potential-dependent in situ Raman spectroscopy to probe the variations in the chemical structure of the as-prepared samples. For Ni|Fe-[TA]-SURMOFs, ex situ Raman peaks are observed at around 1611, 1426, 1136, and 862 cm^{-1} (Figure S13), which are the characteristic features of coordinated organic linkers in pristine SURMOFs.[14] These peaks disappeared after the immersion for 3 min in 0.1 M CsOH, indicating the breaking of coordination bonds between the metal nodes and the organic linkers. A minor peak at $\approx$1642 cm^{-1} is attributed to the uncoordinated carboxylate groups of $[TA]^{2-}$.[14a] Afterward, the in situ Raman spectra were recorded within 400 and 600 cm^{-1} to observe the bending (480 cm^{-1}) and stretching (560 cm^{-1}) vibration modes in NiOOH from 1.20 to 1.70 V vs. RHE (Figures 3a and S14).[7,8,15] One can observe a small peak at $\approx$526 cm^{-1} at 1.20 V vs. RHE in all electrolytes, which is obscured by the Raman signals at $\approx$480 and $\approx$560 cm^{-1} when the applied potential exceeds 1.40 V vs. RHE. The peak at $\approx$526 cm^{-1} could be assigned to the Fe–O vibration in FeOOH.[16] These results indicate that the top layer Fe-[TA] in the pristine SURMOFs was initially derived into FeOOH during the alkali electrolyte immersion and hereafter underwent a re-distribution of Ni and Fe species under the electrochemical treatment. The formed peaks at $\approx$480 and $\approx$560 cm^{-1} reveal the generation of γ-NiOOH species in high oxidation states (+3.3 to +3.7).[17] The additional broad features at 850–1200 cm^{-1} represent the vibration mode of the O–O bond in the active oxygen intermediate $NiOO^-$ (Figure S15).[8,15] The signal appears at potentials of 1.40 V vs. RHE and higher, similar

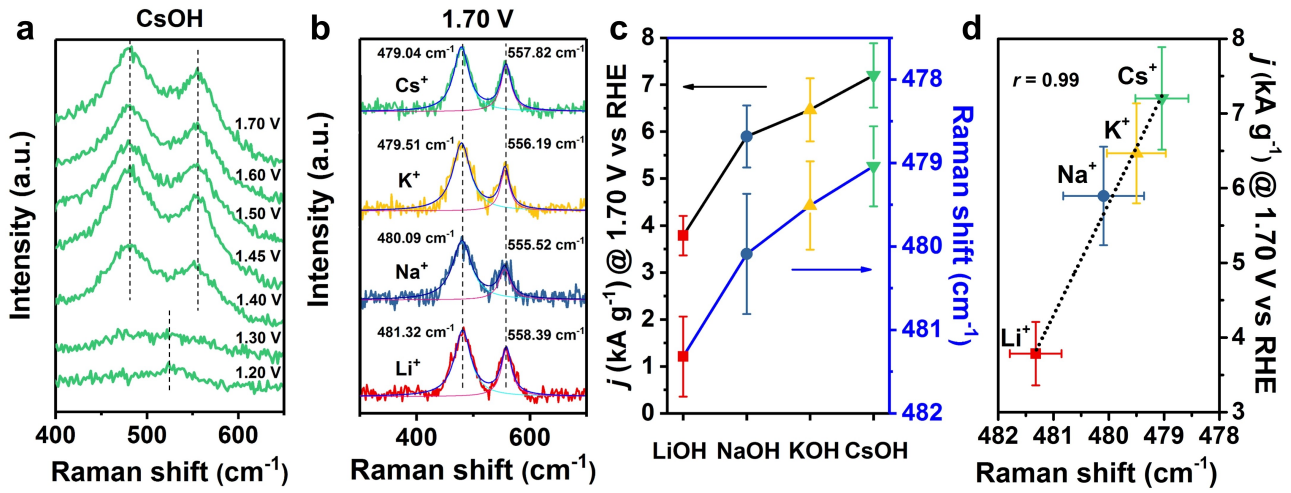

Figure 3. In situ Raman spectroscopy. a) Potential-dependent in situ Raman spectra of the Ni | Fe-[TA]-Catalyst recorded in 0.1 M CsOH electrolyte within a wavenumber range of 400 to 600 cm^{-1}. b) In situ Raman spectra of Ni | Fe-[TA]-Catalyst measured at 1.70 V vs RHE in the presence of different cations. To obtain a more precise peak position, Raman spectra within the range of 300 to 700 cm^{-1} were fitted with Gaussian functions. There are two well-defined Raman peaks at around 480 and 560 cm^{-1}, corresponding to the binding and stretching vibration of Ni–O in NiOOH. c, d) Correlation of the electrocatalytic activities acquired at 1.70 V vs. RHE (solid black line in c) and the Raman peaks at around 480 cm^{-1} (the solid blue line in c) in varying electrolytes. The Pearson correlation coefficient (*r*) is 0.99 according to the linear fitting in d.

to the bending and stretching vibration modes for NiOOH. Figure 3b shows two broad vibration features at 1.70 V vs RHE in all electrolytes. All spectra were fitted according to a Gaussian function to accurately acquire the Raman shifts attributed to the Ni–O vibration modes. We find that the Raman shifts in CsOH appear at ca. 479.04 and 557.82 cm^{-1}, whereas the same features can be observed in LiOH at ca. 481.32 and 558.39 cm^{-1}, respectively, corresponding to an apparent positive shift. Moreover, the cation-dependent Raman shifts for the Ni–O bending from Cs^+ to Li^+ are inversely correlated with the trend of mass activities acquired at 1.70 V vs. RHE (Figure 3c and d). A similar result has been obtained by Koper et al.[8] for a NiOOH catalyst, where the same feature in the presence of Cs^+ appeared at a lower Raman shift (480.1 cm^{-1}) in comparison to other cations, which can be attributed to a longer Ni–O bond. In addition, they proposed that Cs^+ with the biggest ion size can interact with the Ni–OO^- species and enhance the stability of the Ni–OO^--Cs^+ intermediate, leading to a higher catalytic activity.

Furthermore, density functional theory (DFT) calculations have been provided to verify the catalytic activity trend in the presence of different alkali metal cations. As shown in Table S5, the alkali metal cations significantly affect the oxygen surrounding them, both the water molecules in the hydrated layer and the lattice oxygen on the catalyst surface. The coordination bond length variations from Li^+ to Cs^+ are consistent with increased catalytic activities in different electrolytes. This result further clarifies that cations enable to impact the structure of the interfacial water molecules through non-covalent interactions. The presence of a large number of oxygen vacancies in the SURMOF-derived NiFe-(OOH) catalysts has been reported in our previous work and that of others.[3c,18] The oxygen vacancies are pivotal for the OER process. Therefore, DFT calculations were carried out based on the oxygen vacancy in a NiFe(OOH) model. As a multi-electron transfer reaction, the formation or decomposition of the OOH intermediate in OER is usually considered as the rate-determining step (RDS), which represents the transition state with the highest free energy for the whole reaction.[19] With this in mind, we carefully studied the energy required for the adsorption of OH species on a Ni(Fe)O intermediate in the presence of various alkali metal cations, as shown in Figure S17. The catalytic activities increase in the same order as the adsorption energies from Li^+ to Cs^+, which suggests that hydrated cations are able to alter the adsorption energy and thus affect the formation rate of the key reaction intermediate OOH.

For the in situ analysis of the electrode/electrolyte interface, LICT was chosen.[9] In the LICT setup (Figure 4a), an Nd:YAG laser is used to emit short laser pulses with a 5–8 ns pulse duration at a wavelength of 532 nm. The energy of the laser beam was fixed to ca. 12.5 mJ cm^{-2} by an attenuator to avoid possible damage to the electrode. The laser irradiation on the electrode surface results in a temperature jump, inducing the formerly well-oriented water dipoles in the EDL into a disordered state. Subsequently, as a result of the quick relaxation, sharp positive or negative current transients can be observed, as is schematically shown in Figure 4a. Specifically, the PME can be measured using this temporary laser-induced temperature perturbation.[20] The PME is a critical parameter to assess the EDL structure and reflects interfacial energy barriers for electrochemical reactions, e.g., mass and charge transfers.[10a,21] In general, the degree of disorder of the interfacial water layer reaches its maximum at a potential close to the PME. In contrast, the network of water molecules near the charged electrode surface is rigid at potentials far from the PME.[9a,20b] Consequently, it is easier for the reaction species to reach

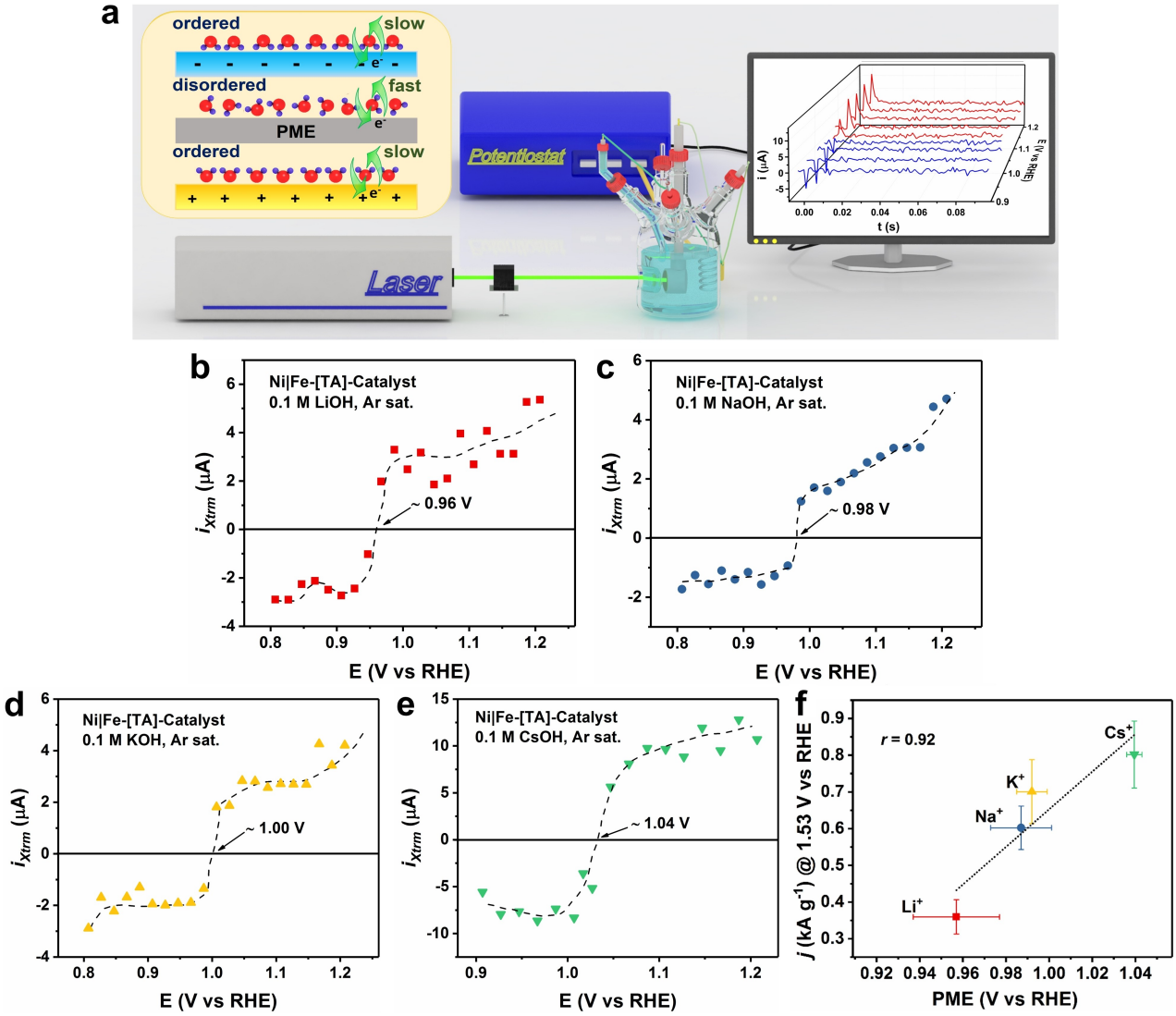

Figure 4. LICT measurements. a) Schematic drawing of the LICT setup used to determine the potential of maximum entropy (PME) for the Ni | Fe-[TA]-Catalyst in Ar-saturated 0.1 M MOH electrolytes. The cell was equipped with a quartz laser transparent window (∅ = 30 mm), a QCM chip fixed in a PTFE holder as a working electrode, a Hg/HgO (1.0 M NaOH) reference electrode, and a Pt wire as a counter electrode. The inset shows the orientation of water dipoles at the charged electrode surface. Note that a state of maximum disorder for water dipoles at the electrode surface can be found at a specific potential, defined as the PME. The temporary temperature increase from the laser illumination of the electrode surface leads to the disruption in the order of surface adsorbed water dipoles. The computer monitor displays the LICT results for Ni | Fe-[TA]-Catalyst in 0.1 M CsOH within the potential range from 0.81 to 1.21 V vs. RHE. b)–e) 2D LICT data representing the correlation of extrema of the current transients and the applied potential in Ar-saturated 0.1 M MOH electrolytes. f) Dependence of the electrocatalytic activities at 1.53 V vs. RHE on the potential of maximum entropy for Ni | Fe-[TA]-Catalyst electrode in the presence of different cations. Herein, the Pearson correlation coefficient (*r*) is 0.92 according to the linear fitting.

the active sites at potentials close to the PME. Thus, one can assume that the closer the PME is to the thermodynamic equilibrium potential of the OER, the faster the OER will be.

With this in mind, the LICT method was conducted to reveal the impact of the cations on the OER performance. In Figure 4b–e, the extreme values of the sharp positive and negative current transients are shown, acquired from the 3D LICT plots (e.g., in Figures 4a and S18). These current response plots represent the orientation of the water dipoles and the excess charge of the electrode surface in the relaxation time frame after the laser illumination.[21] With increasing potential, the signs of the current transients change from negative to positive, corresponding to the sign inversion of the net surface charge at the interface of electrodes, i.e., the change in orientation of the interfacial water molecules. At the PME, the interfacial water layer is already at its maximum disorder. This is when the current transient vanishes, or in other words, the point of transition from negative to positive current transient. This implies that, at the PME, the rearrangement of the interfacial water molecules is facilitated, which is favorable for the interfacial

charge transfers during the catalytic reaction. The trends of the PME for the various electrolytes are presented in Figure 4b–e, where CsOH exhibits the most positive PME at ≈1.04 V vs. RHE compared to the other cation electrolytes. It directly indicates that the PMEs are tightly related to the electrolyte compositions. In this case, having a PME value closer to the theoretical potential (1.23 V vs. RHE) of the OER indicates looser interfacial water molecules, which is conducive to achieving a faster reaction rate. Moreover, the linear dependence of the OER activity on the PMEs for different cations is visible in Figure 4f. The results of the LICT measurements complement the electrochemical and Raman spectroscopy measurements, highlighting the influence of the electrolyte cations on the OER activity of the catalysts.

In summary, we investigated the electrolyte cation effect on the oxygen evolution activity of SURMOF-derived NiFe-(OOH)-based electrocatalysts in different alkali metal hydroxide electrolytes. It was found that the OER activity is sensitive to the alkali metal cations, with the following order: $Cs^+ > K^+ > Na^+ > Li^+$. The in situ Raman spectra support that the catalytic activity is closely associated with the variable-length of Ni–O bonds in the NiOOH active-phase structure. In effect, the enhanced stability of OER intermediates can be induced via the interaction between the large alkali metal cation and the charged intermediate. Further, a perspective in terms of the double-layer order/disorder was introduced into the study of cation effects using the LICT technique. The cation-dependence of the OER activity is in line with the trend of the PMEs, revealing the fact that large Cs^+ cations can significantly affect the structure of the interfacial water layer so that it improves the kinetics of the oxygen evolution reaction. For future studies, the results should be transferable from the special kind of Metal(OOH)-type electrocatalyst using the "SUR-MOF"-strategy to other systems, which feature the same catalytically active key species. Although it remains so far difficult to unveil the most intrinsic role of cations, this work offers further insights into the understanding of the role of the electrode/electrolyte interface in the engineering of cutting-edge electrocatalytic systems.

Acknowledgements

Financial support from DFG projects BA 5795/4-1, BA 5795/5-1, and BA5795/6-1 (in the framework of the DFG research group 2982, UNODE) is gratefully acknowledged. We also appreciate the financial support from Deutsche Forschungsgemeinschaft under Germany's excellence strategy—EXC 2089/1—390776260, Germany's excellence cluster "e-conversion" and the DFG project MOFMOX (FI 502/43-1). S.H. and X.D. acknowledge the financial support from the China Scholarship Council. Open Access funding enabled and organized by Projekt DEAL.

Conflict of Interest

The authors confirm they do not have any conflicts of interest regarding this manuscript.

Data Availability Statement

The data that support the findings of this study are available from the corresponding author upon reasonable request.

Keywords: Cation Effect · Laser-Induced Current Transient · Oxygen Evolution Reaction · Raman Spectroscopy · Surface-Mounted Metal–Organic Frameworks

[1] a) I. Roger, M. A. Shipman, M. D. Symes, *Nat. Chem. Rev.* **2017**, *1*, 0003; b) Q. Zhang, E. Uchaker, S. L. Candelaria, G. Cao, *Chem. Soc. Rev.* **2013**, *42*, 3127–3171; c) T. R. Cook, D. K. Dogutan, S. Y. Reece, Y. Surendranath, T. S. Teets, D. G. Nocera, *Chem. Rev.* **2010**, *110*, 6474–6502.

[2] a) K. Kusada, D. Wu, T. Yamamoto, T. Toriyama, S. Matsumura, W. Xie, M. Koyama, S. Kawaguchi, Y. Kubota, H. Kitagawa, *Chem. Sci.* **2019**, *10*, 652–656; b) L. Francàs, S. Corby, S. Selim, D. Lee, C. A. Mesa, R. Godin, E. Pastor, I.E. L. Stephens, K.-S. Choi, J. R. Durrant, *Nat. Commun.* **2019**, *10*, 5208; c) G. Huang, L. Yang, Q. Yin, Z. B. Fang, X. J. Hu, A. A. Zhang, J. Jiang, T. F. Liu, R. Cao, *Angew. Chem. Int. Ed.* **2020**, *59*, 4385–4390; *Angew. Chem.* **2020**, *132*, 4415–4420; d) E. M. Miner, T. Fukushima, D. Sheberla, L. Sun, Y. Surendranath, M. Dincă, *Nat. Commun.* **2016**, *7*, 10942.

[3] a) W. Li, S. Watzele, H. A. El-Sayed, Y. Liang, G. Kieslich, A. S. Bandarenka, K. Rodewald, B. Rieger, R. A. Fischer, *J. Am. Chem. Soc.* **2019**, *141*, 5926–5933; b) W. Li, S. Xue, S. Watzele, S. Hou, J. Fichtner, A. L. Semrau, L. Zhou, A. Welle, A. S. Bandarenka, R. A. Fischer, *Angew. Chem. Int. Ed.* **2020**, *59*, 5837–5843; *Angew. Chem.* **2020**, *132*, 5886–5892; c) S. Hou, W. Li, S. Watzele, R. M. Kluge, S. Xue, S. Yin, X. Jiang, M. Döblinger, A. Welle, B. Garlyyev, M. Koch, P. Müller-Buschbaum, C. Wöll, A. S. Bandarenka, R. A. Fischer, *Adv. Mater.* **2021**, *33*, 2103218.

[4] a) M. Liu, L. Kong, X. Wang, J. He, J. Zhang, J. Zhu, X.-H. Bu, *Nano Res.* **2021**, *14*, 4680–4688; b) Z. Xiao, Y. Mei, S. Yuan, H. Mei, B. Xu, Y. Bao, L. Fan, W. Kang, F. Dai, R. Wang, L. Wang, S. Hu, D. Sun, H.-C. Zhou, *ACS Nano* **2019**, *13*, 7024–7030; c) H. Zhang, B. Xu, H. Mei, Y. Mei, S. Zhang, Z. Yang, Z. Xiao, W. Kang, D. Sun, *Small* **2019**, *15*, 1904663; d) J. Tian, F. Jiang, D. Yuan, L. Zhang, Q. Chen, M. Hong, *Angew. Chem. Int. Ed.* **2020**, *59*, 13101–13108; *Angew. Chem.* **2020**, *132*, 13201–13208.

[5] J. Zaffran, M. B. Stevens, C. D. M. Trang, M. Nagli, M. Shehadeh, S. W. Boettcher, M. Caspary Toroker, *Chem. Mater.* **2017**, *29*, 4761–4767.

[6] a) D. Strmcnik, K. Kodama, D. van der Vliet, J. Greeley, V. R. Stamenkovic, N. M. Marković, *Nat. Chem.* **2009**, *1*, 466–472; b) S. K. Searles, I. Dzidic, P. Kebarle, *J. Am. Chem. Soc.* **1969**, *91*, 2810–2811; c) B. Garlyyev, S. Xue, M. D. Pohl, D. Reinisch, A. S. Bandarenka, *ACS Omega* **2018**, *3*, 15325–15331; d) B. Huang, K. H. Myint, Y. Wang, Y. Zhang, R. R. Rao, J. Sun, S. Muy, Y. Katayama, J. Corchado Garcia, D. Fraggedakis, J. C. Grossman, M. Z. Bazant, K. Xu, A. P. Willard, Y. Shao-Horn, *J. Phys. Chem. C* **2021**, *125*, 4397–4411; e) J. Mähler, I. Persson, *Inorg. Chem.* **2012**, *51*, 425–438.

[7] J. D. Michael, E. L. Demeter, S. M. Illes, Q. Fan, J. R. Boes, J. R. Kitchin, *J. Phys. Chem. C* **2015**, *119*, 11475–11481.

[8] A. C. Garcia, T. Touzalin, C. Nieuwland, N. Perini, M. T. M. Koper, *Angew. Chem. Int. Ed.* **2019**, *58*, 12999–13003; *Angew. Chem.* **2019**, *131*, 13133–13137.
[9] a) D. Scieszka, J. Yun, A. S. Bandarenka, *ACS Appl. Mater. Interfaces* **2017**, *9*, 20213–20222; b) D. Scieszka, C. Sohr, P. Scheibenbogen, P. Marzak, J. Yun, Y. Liang, J. Fichtner, A. S. Bandarenka, *ACS Appl. Mater. Interfaces* **2018**, *10*, 21688–21695; c) T. C. Nagaiah, A. Tiwari, M. Kumar, D. Scieszka, A. S. Bandarenka, *ACS Appl. Energy Mater.* **2020**, *3*, 9151–9157.
[10] a) I. Ledezma-Yanez, W. D. Z. Wallace, P. Sebastián-Pascual, V. Climent, J. M. Feliu, M. T. M. Koper, *Nat. Energy* **2017**, *2*, 17031; b) R. Subbaraman, D. Tripkovic, D. Strmcnik, K. C. Chang, M. Uchimura, A. P. Paulikas, V. Stamenkovic, N. M. Markovic, *Science* **2011**, *334*, 1256–1260; c) Y. Marcus, *Chem. Rev.* **2009**, *109*, 1346–1370; d) N. Garcia-Araez, V. Climent, J. Feliu, *J. Phys. Chem. C* **2009**, *113*, 9290–9304.
[11] S. Zhao, Y. Wang, J. Dong, C.-T. He, H. Yin, P. An, K. Zhao, X. Zhang, C. Gao, L. Zhang, J. Lv, J. Wang, J. Zhang, A. M. Khattak, N. A. Khan, Z. Wei, J. Zhang, S. Liu, H. Zhao, Z. Tang, *Nat. Energy* **2016**, *1*, 16184.
[12] W. Zheng, M. Liu, L. Y. S. Lee, *ACS Catal.* **2020**, *10*, 81–92.
[13] a) Q. Gao, C. Ranjan, Z. Pavlovic, R. Blume, R. Schlögl, *ACS Catal.* **2015**, *5*, 7265–7275; b) J. Suntivich, E. E. Perry, H. A. Gasteiger, Y. Shao-Horn, *Electrocatalysis* **2013**, *4*, 49–55.
[14] a) W. Li, F. Li, H. Yang, X. Wu, P. Zhang, Y. Shan, L. Sun, *Nat. Commun.* **2019**, *10*, 5074; b) J. Chen, P. Zhuang, Y. Ge, H. Chu, L. Yao, Y. Cao, Z. Wang, M. O. L. Chee, P. Dong, J. Shen, M. Ye, P. M. Ajayan, *Adv. Funct. Mater.* **2019**, *29*, 1903875.
[15] S. Lee, L. Bai, X. Hu, *Angew. Chem. Int. Ed.* **2020**, *59*, 8072–8077; *Angew. Chem.* **2020**, *132*, 8149–8154.
[16] a) Z. Qiu, C.-W. Tai, G. A. Niklasson, T. Edvinsson, *Energy Environ. Sci.* **2019**, *12*, 572–581; b) D. L. A. de Faria, S. Venâncio Silva, M. T. de Oliveira, *J. Raman Spectrosc.* **1997**, *28*, 873–878.
[17] a) B. S. Yeo, A. T. Bell, *J. Phys. Chem. C* **2012**, *116*, 8394–8400; b) S. Klaus, Y. Cai, M. W. Louie, L. Trotochaud, A. T. Bell, *J. Phys. Chem. C* **2015**, *119*, 7243–7254.
[18] S. Zhao, C. Tan, C.-T. He, P. An, F. Xie, S. Jiang, Y. Zhu, K.-H. Wu, B. Zhang, H. Li, J. Zhang, Y. Chen, S. Liu, J. Dong, Z. Tang, *Nat. Energy* **2020**, *5*, 881–890.
[19] K. S. Exner, *Chem Catalysis* **2021**, *1*, 258–271.
[20] a) V. Climent, B. A. Coles, R. G. Compton, *J. Phys. Chem. B* **2002**, *106*, 5988–5996; b) N. García-Aráez, V. Climent, J. M. Feliu, *J. Am. Chem. Soc.* **2008**, *130*, 3824–3833.
[21] V. Climent, B. A. Coles, R. G. Compton, *J. Phys. Chem. B* **2001**, *105*, 10669–10673.

Manuscript received: January 31, 2022
Accepted manuscript online: March 10, 2022
Version of record online: April 19, 2022